analytical chemistry

pubs.acs.org/ac Article

Assessing Accuracy of an Analytical Method *In Silico*: Application to "Accurate Constant via Transient Incomplete Separation" (ACTIS)

Jean-Luc Rukundo, J. C. Yves Le Blanc, Sven Kochmann, and Sergey N. Krylov*

Cite This: *Anal. Chem.* 2020, 92, 11973−11980 Read Online

ACCESS | Metrics & More | Article Recommendations | Supporting Information

ABSTRACT: Analytical methods may not have reference standards required for testing their accuracy. We postulate that the accuracy of an analytical method can be assessed in the absence of reference standards *in silico* if the method is built upon deterministic processes. A deterministic process can be precisely computer-simulated, thus allowing virtual experiments with virtual reference standards. Here, we apply this *in silico* approach to study "Accurate Constant via Transient Incomplete Separation" (ACTIS), a method for finding the equilibrium dissociation constant (K_d) of protein−small-molecule complexes. ACTIS is based on a deterministic process: molecular diffusion of the interacting protein−small-molecule pair in a laminar pipe flow. We used COMSOL software to construct a virtual ACTIS setup with a fluidic system mimicking that of a physical ACTIS instrument. Virtual ACTIS experiments performed with virtual samples—mixtures of a protein and a small molecule with defined rate constants and, thus, K_d of their interaction—allowed us to assess ACTIS accuracy by comparing the determined K_d value to the input K_d value. Further, the influence of multiple system parameters on ACTIS accuracy was investigated. Within multifold ranges of parameter values, the values of K_d did not deviate from the input K_d values by more than a factor of 1.25, strongly suggesting that ACTIS is intrinsically accurate and that its accuracy is robust. Accordingly, further development of ACTIS can focus on achieving high reproducibility and precision. We foresee that *in silico* accuracy assessment, demonstrated here with ACTIS, will be applicable to other analytical methods built upon deterministic processes.

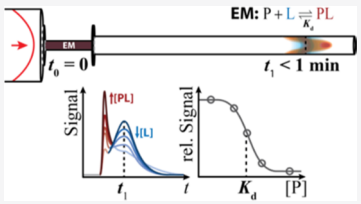

Accuracy is one of the key performance parameters of quantitative analytical methods. Many methods do not have reference standards and, thus, their accuracy cannot be experimentally tested. We suggest that the accuracy of an analytical method can be assessed in the absence of reference standards *in silico* if the underlying physicochemical processes are deterministic, i.e., can be precisely simulated. Detailed computer simulation should facilitate virtual experiments in which a virtual sample can be perfectly defined and, thus, can serve as a virtual reference standard. In this work, we applied this *in silico* accuracy assessment to "Accurate Constant via Transient Incomplete Separation (ACTIS)".

ACTIS is a separation-based method for finding K_d of complexes (PL) between proteins (P) and small-molecule ligands (L). Such reversible binding of proteins to small-molecule ligands plays an important role in the regulation of cellular processes as well as in drug development since most therapeutic targets are proteins and most drugs are small molecules[1]

$$\mathrm{P} + \mathrm{L} \underset{k_{off}}{\overset{k_{on}}{\rightleftarrows}} \mathrm{PL} \tag{1}$$

where K_d is defined via equilibrium concentrations of P, L, and PL

$$K_d = [\mathrm{L}]_{eq}[\mathrm{P}]_{eq}/[\mathrm{PL}]_{eq} \tag{2}$$

There is no reference standard for the determination of K_d, i.e., there is no PL with a known K_d; thus, the accuracy of ACTIS cannot be assessed experimentally. On the other hand, ACTIS is built upon a deterministic process of molecular diffusion of P, L, and PL, interacting as in eq 1 while moving within a laminar pipe flow. This process can be precisely described by a set of partial differential equations with precisely defined initial and boundary conditions (see the Supporting Information) and precisely defined input values of the rate constants in eq 1 ($k_{on,inp}$ and $k_{off,inp}$) for computer simulation. The input values of the rate constants define the input value of the equilibrium constants

$$K_{d,inp} = k_{off,inp}/k_{on,inp} \tag{3}$$

which can serve as a virtual reference standard in virtual ACTIS experiments. Accordingly, ACTIS is suitable for *in silico* accuracy assessment.

In ACTIS, a short plug of an equilibrium mixture of P and L in a buffer solution is injected into a capillary prefilled with the pure buffer solution. The plug is then propagated inside the capillary by a pressure-driven flow of the buffer solution. Different rates of transverse diffusion of PL and L in laminar

Received: June 5, 2020
Accepted: August 3, 2020
Published: August 3, 2020

https://dx.doi.org/10.1021/acs.analchem.0c02405
Anal. Chem. 2020, 92, 11973−11980

flow cause their transient incomplete separation (TIS) (Figure 1A) resulting in a nondiffusive peak for PL and a diffusive peak

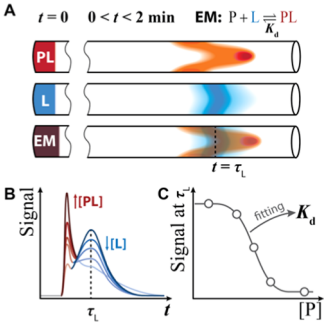

Figure 1. Simplified schematic of determining K_d by ACTIS. (A) Short plug of the equilibrium mixture (EM) of P and L is propagated through a capillary. Differences in the transverse diffusion of PL and L cause their longitudinal separation. (B) Longitudinal separation results in two peaks, and a cumulative signal from L and PL is measured at time τ_L, which is the characteristic time of the transverse diffusion of L. The signal is measured at a constant concentration of L and varying concentrations of P. (C) Binding isotherm "signal-at-τ_L vs concentration of P" is built, and K_d is found by fitting the binding isotherm with eq 7.

for L (Figure 1B). To determine K_d, TIS is performed for a series of equilibrium mixtures with a constant concentration of L and varying concentration of P, producing a set of curves termed separagrams (Figure 1B). The cumulative signal of protein-bound L and unbound L is taken at the time corresponding to the maximum of the diffusive peak for each curve. Subsequently, a classical binding isotherm "signals vs concentration of P" is built to reveal the value of K_d (Figure 1C). ACTIS is a uniquely deterministic method as it relies on molecular diffusion in a pressure-driven flow, which can be described by a system of partial differential equations with fully defined initial and boundary conditions.[1−3] As such, it is perfectly suited for the computational assessment of its accuracy.

A physical ACTIS instrument has a minimum fluidic system with a pump, an injection loop, a separation capillary, and a multiport valve (Figure 2A).[1−3] The valve serves as two connectors: one from a pump tube to the injection loop and the other one from the injection loop to the separation capillary. Accordingly, the instrument has five essential fluidic components, which can be presented as a series of coaxial pipes of different radii (Figure 2B). We used COMSOL to construct a five-component ACTIS setup depicted in Figure 2B with dimensions identical to those of a physical ACTIS instrument (described in the figure legend). We found that K_d determined in this setup deviated from $K_{d,inp}$, defined by eq 3 and used as a virtual reference standard, by a factor of 1.02. This setup was utilized to study how the accuracy of K_d was affected by variations in (i) the radius of the injection loop while keeping its volume constant, (ii) the radius of the separation capillary, (iii) the shape of the initial (prior to the start of TIS) plug of the equilibrium mixture, and (iv) the ramp time in the flow rate onset (after the start of TIS). The variations of parameter values used in this study exceeded markedly those that are expected in a physical ACTIS setup. We found that despite multifold variations in values of a number of parameters, the maximum deviation of K_d from $K_{d,inp}$ was less than a factor of 1.25, suggesting a robust intrinsic accuracy of ACTIS.

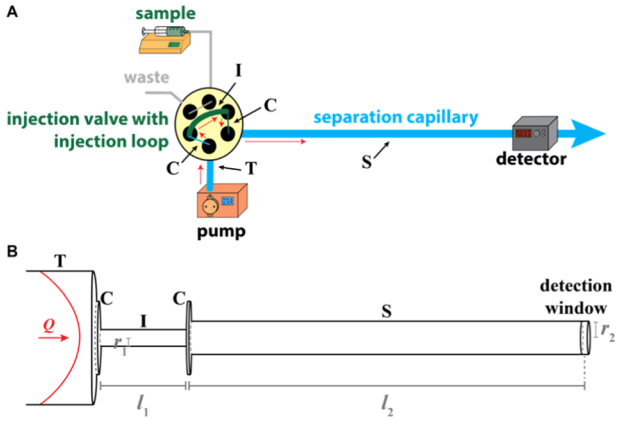

Figure 2. Schematics of a physical (A) and computational (B) ACTIS instrument. The four letters (T, I, S, and C) label the five components simulated in this study and their respective physical counterparts with default dimensions: pump tube (T, 5-cm length, 400-μm radius), injection loop (I, l_1 = 13 cm, r_1 = 50 μm), separation capillary (S, l_2 = 50 cm, r_2 = 100 μm) with a detection window (5-mm length, 100-μm radius) at the end, and two identical connectors (C, 1.1-mm length, 220-μm radius) linking T to I and I to S. Q is the volumetric flow rate provided by a virtual pump. Flow rates were different during sample injection from the loop into the capillary (Q_{inj} = 5 μL/min) and during the following TIS stage (Q_{TIS} = 50 μL/min). Q_{inj} and Q_{TIS} were not varied in this study. By default, the switch between Q_{inj} and Q_{TIS} was set to 10 ms.

The intrinsic accuracy of ACTIS has great practical importance as it allows ACTIS developers to vary the instrument configuration without raising concerns about the influence of such variations on the accuracy of K_d. Efforts and resources can thus be focused on optimizing the instrument configuration to achieve the best reproducibility and the highest precision, the second most important performance parameter of this quantitative analytical method.

■ THEORETICAL BACKGROUND

Here we describe the theoretical aspects of ACTIS that are essential for understanding this method at the conceptual level and help establish the theoretical background required for understanding our current work. In particular, we explain the basic principles of K_d determination and TIS of L from PL; the corresponding two sections are a close reiteration of our previously published explanation.[1]

General Procedure of K_d Determination. In general, finding K_d requires the determination of a fraction R of unbound L in the equilibrium mixture of L and P with the initial concentrations $[L]_0$ and $[P]_0$, respectively

$$R = [L]_{eq}/[L]_0 \tag{4}$$

Finding R, in turn, requires a signal S that is a superposition of signals from L and PL

$$S = S_L \times R + S_{PL} \times (1 - R), \quad S_L \neq S_{PL} \tag{5}$$

where S_L and S_{PL} are the signals of pure L ($[L] = [L]_0$, $[PL] = 0$) and pure PL ($[L] = 0$, $[PL] = [L]_0$), respectively; S_L and S_{PL} can be found in experiments with $[P]_0 = 0$ and $[L]_0 \ll [P]_0 \gg K_d$, respectively. The signal from pure P must be negligible with respect to S shown in eq 5 even for $[L]_0 \ll [P]_0 \gg K_d$. It should be noted that this requirement does not impose a serious practical limitation for ACTIS. In fact, this requirement is common for all titration methods measuring the

https://dx.doi.org/10.1021/acs.analchem.0c02405
Anal. Chem. 2020, 92, 11973−11980

concentration of the unreacted analyte (L in our case) as a function of the total concentration of the titrant (P in our case): the signal of the unreacted titrant should be negligible with respect to that of the analyte. Both fluorescent detection of a fluorescently labeled L and mass-selective detection of L (after complex dissociation) with MS can facilitate satisfying this requirement.

From eq 5, R can be experimentally determined via measuring three signals, S_L, S_{PL}, and S, and using the following expression

$$R_{exp} = (S - S_{PL})/(S_L - S_{PL}) \tag{6}$$

R can be also expressed theoretically as a function of K_d, $[P]_0$, and $[L]_0$[1,4]

$$R_{theor} = -\frac{K_d + [P]_0 - [L]_0}{2[L]_0} + \sqrt{\left(\frac{K_d + [P]_0 - [L]_0}{2[L]_0}\right)^2 + \frac{K_d}{[L]_0}} \tag{7}$$

Then, a standard way of finding K_d is to determine R_{exp} for a wide range of $[P]_0$ at a constant $[L]_0$ and to plot a binding isotherm: R_{exp} vs $[P]_0$. Finally, this binding isotherm is fitted with eq 7 using K_d as a fitting parameter and the best fit reveals the sought value of K_d.[1]

Fundamentally, finding R_{exp} with eq 6 requires that S_L and S_{PL} be measurable and that $S_L \neq S_{PL}$. The latter inequality of signals from pure L and pure PL requires that L and PL be "separated" either spectrally or physically.[5] Importantly, complete separation is not required if a signal from the mixture of L and PL is a superposition of signals from individual components L and PL comprising the mixture (see eq 5) and if pure P does not contribute to the cumulative signal from L and PL. As a result, spectral methods that provide only incomplete separation of signals from L and PL (optical spectra of L and LP do overlap typically) are common in finding R_{exp}.[5−7] ACTIS facilitates finding R_{exp} via incomplete physical separation of L and PL.

Transient Incomplete Separation of L from PL. TIS of L from PL will occur always when a short plug of their mixture is propagated within a Hagen−Poiseuille laminar flow in a long capillary. Such a flow is established by a pressure difference between the capillary ends and has a characteristic parabolic profile of flow velocity: the velocity ranges from zero at the capillary walls to its maximum in the capillary center.[8] TIS of L from PL in the longitudinal direction is possibly due to the difference in rates of transverse diffusion between small-sized L and large-sized PL. PL that is near the capillary center will diffuse to the capillary wall slower than L and, thus, will be displaced longitudinally by the flow more than L. PL located near the capillary wall will diffuse to the capillary center slower than L and will be displaced longitudinally by the flow less than L. As a result, during a short transitional stage, a bulk of PL moves faster than a bulk of L, while a tail of PL moves slower than that of L. The separation is incomplete, i.e., the longitudinal concentration profiles (concentration vs position in the capillary) of L and PL do overlap, even during the transitional stage. Further, this separation gradually dissipates, i.e., the longitudinal concentration profiles of L and PL become symmetrical around the same symmetry axis, after the transitional stage. The after-TIS stage is described by the well-known Taylor dispersion.[9]

Tracking TIS is viewed to be optimal with a flow system in which the optimum distance from the starting position of the equilibrium mixture plug to the detector (l_{opt}) is linked with the average flow velocity (v_{av}), the characteristic time of the transverse diffusion of L from the center of the capillary to its inner wall (τ_L), the volumetric flow rate (Q), and the diffusion coefficient of L (μ_L), as follows[1,10]

$$l_{opt} = v_{av}\tau_L = Q/(\pi\mu_L) \tag{8}$$

where v_{av} relates to Q and the inner capillary radius (r) as

$$v_{av} = Q/(\pi r^2) \tag{9}$$

The characteristic time of transverse diffusion across the capillary is defined in general as

$$\tau = r^2/\mu \tag{10}$$

Longitudinal concentration profiles of L and PL are partially separated in the time domain as shown in Figure 1B. Further, if a signal can be measured for each of L and PL, with the above-mentioned detector, inside the capillary or at its exit and is proportional to the average cross-sectional concentration of each of them, $S_L \propto [L]$ and $S_{PL} \propto [PL]$, then, the cumulative signal S satisfies eq 5 and can, thus, be used to determine R_{exp} with eq 6. Finally, R_{exp} can be measured for a wide range of $[P]_0$ to construct a classical binding isotherm R_{exp} vs $[P]_0$, which, in turn, can be used to find K_d via fitting the isotherm with eq 7.

■ DESIGNING A VIRTUAL ACTIS EXPERIMENT

Five-Component Virtual ACTIS Setup. The five-component physical ACTIS system depicted in Figure 2A operates as follows. The injection loop is filled with the sample. The sample is slowly transferred into the separation capillary at a distance equal to the sample plug length from the capillary entry. The sample is then propagated fast through the separation capillary to cause TIS of L from PL.

We used COMSOL to construct a virtual five-component ACTIS setup with default dimensions identical to those of a physical ACTIS instrument (Figure 2B). The dimensions of the two connectors are identical and can be considered fixed as well as the dimensions of the pump tube. The dimensions of the injection loop and the separation capillary may need to be changed and, thus, were varied in this study. Of course, the virtual system also contains representations of a virtual pump (a source of a hydrodynamic flow characterized by its volumetric flow rate Q) and a virtual detector (a detection volume inside the capillary), which are also associated with some parameters that can vary and potentially cause inaccuracy in K_d.

A default initial configuration in the virtual five-component setup is the one in which the loop and the loop−capillary connector are filled with the sample, while the remaining components are filled with the buffer solution. This situation mirrors the physical ACTIS setup. In a default virtual ACTIS experiment, the sample is slowly transferred from the injection loop to the separation capillary ($Q = Q_{inj}$) and then propagated fast inside the capillary as in the physical ACTIS experiment ($Q = Q_{TIS}$).

Further in this work, the five-component setup was used first to test the accuracy of K_d for the default geometry (Figure 2B). Then, in a more rigorous study, it was used to investigate how the accuracy of K_d determined with ACTIS was affected by

https://dx.doi.org/10.1021/acs.analchem.0c02405
Anal. Chem. 2020, 92, 11973−11980

variations in (i) the radius of the injection loop while keeping its volume constant, (ii) the radius of the separation capillary, (iii) the shape of the initial (prior to the start of TIS) plug of the equilibrium mixture, and (iv) the ramp time in the flow rate onset (after the start of TIS). Below, we provide details on how these four parts of the study were set up.

Geometry of the Injection Loop and Separation Capillary. There are four parameters that characterize the geometry of the injection loop and the separation capillary: the radius (r_1) and length (l_1) of the injection loop and the radius (r_2) of the separation capillary and the distance from the beginning of the separation capillary to the center of the virtual detector (l_2). We conducted two sets of virtual ACTIS experiments in which r_1 and r_2 were varied. In one set of virtual experiments, r_1 was varied from 5 to 5000 μm (l_1 was changed accordingly to keep the volume of the injection loop constant), while r_2 and l_2 were kept constant at default values linked through eqs 8, 9, and 10. In the other set of virtual experiments, r_2 was varied from 5 to 5000 μm while holding constant r_1, l_1, and l_2. The rest of the parameters were default (see Figure 2B).

Geometry of the Initial Sample Plug. While the ideal shape of the initial plug of the equilibrium mixture at the beginning of the separation capillary is cylindrical, in a real experiment, it will be distorted to some degree due to the imperfections of the injection process. To assess how such distortions can affect the accuracy of K_d, we examined square, Gaussian, and half-Gaussian longitudinal distributions of concentrations of L, PL, and P in the initial plug (Figure 3A); cross-sectional concentration profiles were uniform. Here, as opposed to a default way of injecting a 3.0-cm long sample plug from the injection loop, the same-length initial plug was defined near the entrance of the separation capillary at a distance equal to the plug length, and no injection process was simulated. To model this initial plug shape, the longitudinal (along axis x) distribution of concentrations was defined as a square wave function

$$f(k_1, k_2, x) = H(k_1x/L) - H(k_2x/L - 1) \quad (11)$$

where $H(kx) = 1/(1 + e^{-2kx})$, which is an analytical sigmoidal approximation of the Heaviside step function.[11] The shape of the plug was varied by varying both k_1 and k_2. The condition of $k_1 = k_2$ corresponds to symmetric plug shapes, e.g., for $k_1 = k_2 = 2$, the plug shape is Gaussian and for $k_1 = k_2 = 200$, the plug shape is a close approximation of the square function. For $k_1 \neq k_2$, the plug shape is asymmetric, e.g., half-Gaussians. The rest of the parameters were default (see Figure 2B).

Ramp Time in Flow Rate Onset. Achieving and maintaining the ideal plug shape require the injection of a sample plug from the injection loop into the separation capillary at a slow flow rate of Q_{inj} for a time period of t_{inj}. TIS, on the other hand, requires the propagation of the injected sample plug through the separation capillary at a high flow rate of Q_{TIS}. In a virtual ACTIS experiment, the transition from Q_{inj} to Q_{TIS} can be very fast (e.g., subseconds) or even instant. In a real experiment, however, this transition is a process that requires a second-scale time interval of t_{ramp}, i.e., the ramp time of the flow rate onset (Figure 3B). In ACTIS, the run time is relatively short (peaks of PL and L are detected within 30 s), i.e., the ramp time of a few seconds may significantly influence the TIS of L from PL. Therefore, we varied t_{ramp} to examine the impact of this variation on the profiles of PL and L and, in turn, on the accuracy of K_d determined with ACTIS. The rest of the parameters were default (see Figure 2B).

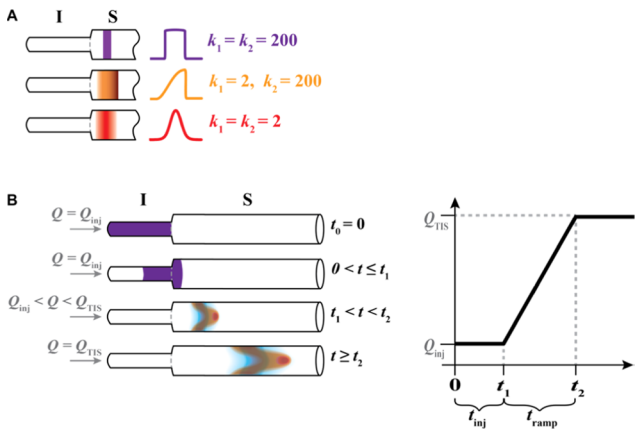

Figure 3. Schematic of the simulated geometries in ACTIS. For clarity, the pump tube (T) and connectors (C) are omitted in the presentations here. (A) Schematic of three different initial plug shapes at the entrance of the separation capillary. Different concentration distributions inside the capillary (left) and longitudinal concentration profiles (result of integration across the capillary, middle) are obtained by changing parameters k_1 and k_2 (right) in the Heaviside function (see the text for details). (B) Schematic showing two key steps in ACTIS: the slow injection of the mixture into the separation capillary and its fast propagation inside the capillary; a transition period required to ramp up the flow rate connects the two stages. The sample plug is injected from the injection loop into the separation capillary for a time period of t_{inj} at a flow rate of Q_{inj}. Immediately after completing the injection, the volumetric flow rate is set to Q_{TIS} and the plug is further propagated through the separation capillary. The time interval required to reach the propagation flow rate Q_{TIS} is t_{ramp}.

SETTING UP A VIRTUAL ACTIS EXPERIMENT IN COMSOL

To simulate TIS in the five-component setup depicted in Figure 2B, we used COMSOL Multiphysics software, version 5.4, with the "transport of diluted species" and "laminar flow" modules, which incorporate equations for both mass transfer and reversible binding of P and L in an equilibrium mixture.

Computation time depends on the dimensions of the simulated geometries; thus, to reduce this time, the lengths of all of the five fluidic components can be scaled down along with the length of the detection window.[1] In such a case, the values of Q_{inj} and Q_{TIS} must also be scaled down to keep the l_2/Q_{TIS} ratio constant. The scaled-down dimensions used in COMSOL computation are reported in the Supporting Information. Moreover, the mesh size was chosen to minimize computational time and memory requirements. For all of the simulations, the "finer mesh" setting in COMSOL was used with a computational time of ≈3 h (2 × Intel Xenon CPU X5690@3.47 GHz, 96 GB RAM); finer settings such as "extra fine mesh" resulted in some cases in a better accuracy (up to 10 times better); however, they required an order of magnitude longer computational time (≈20 h) (Supporting Information).

Choice of Simulation Parameters. ACTIS was introduced as a method for measuring K_d of protein−small-molecule complexes, which play key roles in biology and technology;[1] its application to other interacting pairs is not under consideration at this time. An average molecular weight

https://dx.doi.org/10.1021/acs.analchem.0c02405
Anal. Chem. 2020, 92, 11973−11980

(MW) of eukaryotic proteins is 50 kDa (average length of 450 amino acids), which corresponds to a diffusion coefficient of $\mu_P \approx 50\ \mu m^2/s$;[12] an example of a small protein is cytochrome C with MW = 13 kDa and $\mu_P = 110\ \mu m^2/s$.[13] Small molecules have MW < 1 kDa and $300 \leq \mu_L \leq 1500\ \mu m^2/s$.[14] Thus, the lowest expected ratio of the diffusion coefficients is $\mu_L/\mu_p \approx 3$; this ratio will be a rare case. We thus consider a reasonable "average" case of $\mu_P = 50\ \mu m^2/s$ and $\mu_L = 500\ \mu m^2/s$ ($\mu_L/\mu_p \approx 10$). Separagrams for $\mu_L/\mu_p = 10$ and $\mu_L/\mu_p = 3$ differ somewhat in peak resolution (Figure S1), but this difference does not affect the accuracy in virtual or real experiments provided that the signal-to-noise ratio is high. Therefore, we do not consider variation in μ_L/μ_p as a source of inaccuracy for this study.

ACTIS is designated for probing strong binding interactions, such as those between proteins and therapeutic hits with K_d in the micromolar range or lower. For such strong interactions, k_{off} values are typically below the maximum k_{off} used in this study: $k_{off,inp} = 10^{-3}\ s^{-1}$. In ACTIS, the separation time must be shorter than the characteristic time of complex dissociation ($\approx 1/k_{off}$). As explained above, the separation time in ACTIS is approximately equal to the characteristic time of transverse diffusion, of a molecule with diffusion coefficient μ, across the capillary, with radius r, as defined in eq 10. For a typical $\mu_L = 500\ \mu m^2/s$ and r ranging from 10 to 100 μm, the separation time ranges from 0.2 to 20 s. Experimentally, this would allow studying interactions with k_{off} up to 10 s^{-1}.

In summary, the input parameters used as COMSOL settings were $k_{on,inp} = 10^3\ M^{-1}\ s^{-1}$, $k_{off,inp} = 10^{-3}\ s^{-1}$, $K_d = k_{off,inp}/k_{on,inp} = 10^{-6}\ M^{-1}$, $\mu_{PL} = \mu_P = 50\ \mu m^2/s$, $[L]_0 = 0.5\ \mu M$, and $T = 300$ K. $[P]_0$ was varied from 1 nM to 1 mM using 11 different nonzero concentrations and zero concentration. Three other values of $k_{off,inp}$ i.e., 10^{-4} 10^{-5}, and $10^{-6}\ s^{-1}$ with respective values of $K_{d,inp}$, 10^{-7}, 10^{-8}, and 10^{-9} M, were also used in COMSOL. Testing several k_{off} values allowed us to verify the independence of the simulations on k_{off} and, therefore, K_d; the simulations were shown to be consistent with the default value of $k_{off,inp} = 10^{-3}\ s^{-1}$ (Figure S2).

The sample plug is fully injected during $t_{inj}/2$ ($t_{inj} = 24$ s). Subsequently, the sample plug is displaced from the entrance of the separation capillary inside the capillary at a distance equal to the plug length during another $t_{inj}/2$. This displacement is meant to place the initial plug away from the junction between the loop−capillary connector and the separation capillary; flow disturbance is expected to be the greatest near the junction.

The virtual detector was meant to be at the end of the virtual separation capillary, and virtual detection was performed by averaging concentrations across the capillary within a cylindrical detection window (dimensions: 5 mm × r_2). Experimentally, the cumulative signal S from protein-bound L and unbound L is obtained by averaging points within a time window around the second-peak maximum, i.e., the diffusive peak (around time τ_L in Figure 1B).[1] Using a finite-length time window compensates for noise in experimental data; accordingly, we used a finite time window to find the cumulative signal S for all our virtual experiments. Unless otherwise stated, for all of the separagrams, the position of the time window was chosen by default by selecting the time at which $S_L > S_{PL}$ and $S_L - S_{PL} = \max$.

All of the five fluidic components were modeled as 2D axisymmetric shapes to further reduce computation time in COMSOL.

To study how the variation in the ramp time of flow onset affects the accuracy of K_d, a piecewise function was defined in COMSOL for the linear transition from Q_{inj} to Q_{TIS}, and the length of this transition time, t_{ramp}, was varied.

To study how the variation in plug shape influences the accuracy of K_d, a concentration distribution (eq 11) was defined as an analytical function in COMSOL and, then, varied as explained in the Setting Up a Virtual ACTIS Experiment in COMSOL section.

Note that neither COMSOL nor any other computational calculation software possesses infinite (numerical) accuracy. COMSOL's inaccuracy will contribute to the assessment of ACTIS's inaccuracy, making it an assessment of the lower limit of ACTIS accuracy.

■ RESULTS AND DISCUSSION

General Considerations. In the following, "K_d" refers to the determined K_d values obtained by fitting eq 7 into the respective binding isotherm, while $K_{d,inp}$ (defined by $k_{on,inp}$ and $k_{off,inp}$; see the Choice of Simulation Parameters section) is the K_d value set in the COMSOL simulation. It is difficult to set up a benchmark for K_d accuracy, but taking into account that variations in K_d determined experimentally often reach orders of magnitude, we consider deviation by less than a factor of 1.25 as acceptable. Accordingly, for the purpose of this work, we consider K_d accurate if $0.80 < K_d/K_{d,inp} < 1.25$. We assume that the virtual ACTIS system is stable (this was confirmed by repeating virtual runs); therefore, we do not provide random errors. Note that we do not consider the detector as a source of imprecision in the following consideration because highly precise detectors for different detection methods, such as fluorescence and mass spectrometry, are available. In fact, any detector that can measure a cumulative cross-sectional average signal from L and PL satisfying eq 5 is suitable for accurate ACTIS measurements provided that it satisfies the following requirements. The detector must have a sufficiently high signal readout speed and a concentration limit of quantitation below K_d values of the studied complexes; the limit of quantification (LOQ = 10 × S/N, where N is the level of noise) for L on the used detector should be at least equal to $[L]_0$.[4]

Accuracy of the Default ACTIS Setup. The virtual five-component ACTIS setup, described in the Setting Up a Virtual ACTIS Experiment in COSMOL section, was first examined for accuracy under default conditions shown in Figure 2B. A full set of separagrams was calculated, and K_d was determined from the respective binding isotherm (Figure 4). We found

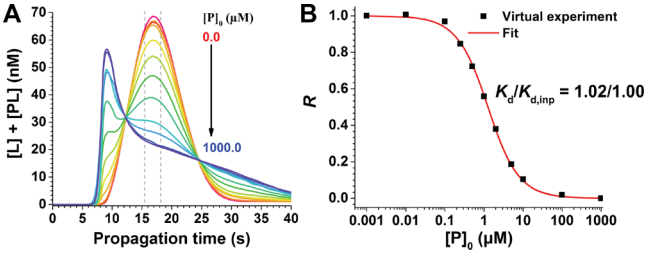

Figure 4. Separagrams (A) and the resulting binding isotherm (B) for a virtual ACTIS experiment in the five-component fluidic system, mimicking a realistic ACTIS setup schematically depicted in Figure 2. The dashed lines indicate the time window within which the average signal was taken to calculate the R_{exp} values using eq 6. The binding isotherm was fit with eq 7 with K_d being a fitting parameter.

https://dx.doi.org/10.1021/acs.analchem.0c02405
Anal. Chem. 2020, 92, 11973−11980

that K_d determined in this setup deviated from $K_{d,inp}$ by a factor of 1.02. The proven accuracy of the default five-component ACTIS setup opened a route for performing a more stringent accuracy test with variations in (i) the radius of the injection loop while keeping its volume constant, (ii) the radius of the separation capillary, (iii) the shape of the initial (prior to the start of TIS) plug of the equilibrium mixture, and (iv) the ramp time in the flow rate transfer from Q_{inj} to Q_{TIS}.

Variation of Injection Loop Radius. In this examination, r_1 was varied from 5 to 5000 μm (the default value for r_1 was 50 μm). This variation in r_1 corresponded to variation in r_1/r_2 from 0.05 (=5/100) to 50 (=5000/100) for the default value of r_2 = 100 μm. To keep the volume of the injection loop constant (which is the purpose of the injection loop), l_1 was changed accordingly for each r_1: $l_1 \sim 1/r_1^2$. The rest of the parameters were default (see Figure 2B).

For each value of r_1, a full set of separagrams has been computed, and the K_d value was determined from a respective binding isotherm (Figure S3). All determined K_d values were compared to $K_{d,inp}$ (Figure 5A). We found that K_d was accurate

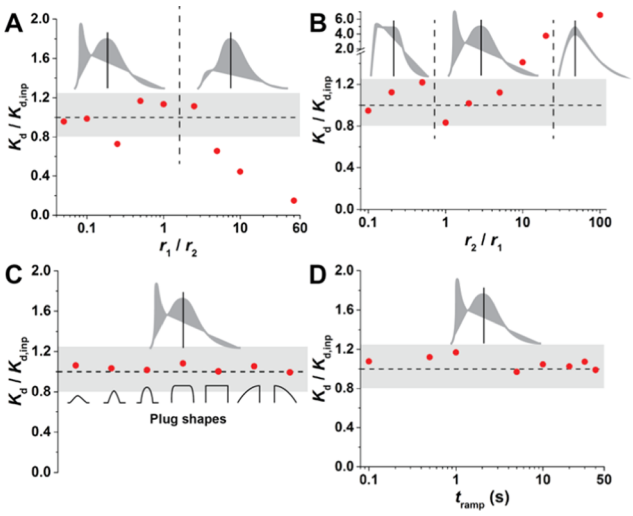

Figure 5. K_d accuracy results of virtual ACTIS experiments by varying (A) injection loop radius (r_1), (B) separation capillary radius (r_2), (C) injection plug shape, and (D) propagation pump ramp time (t_{ramp}). The red dots mark the evaluated relative K_d values. The gray area in each panel marks the range in $K_d/K_{d,inp}$ (from 0.8 to 1.25), which is considered as the "area of accuracy" in this study; the horizontal black dashed line marks the target relative K_d value (1.0). The small separagram figures in each panel show the change of separagram shape when varying the abscissa parameter; the vertical black line indicates the position of the detection window at which the evaluation was done; the shaded areas show the magnitude of change in the ordinate when varying $[P]_0$. See the text and the Supporting Information for more details.

according to our criteria ($0.8 < K_d/K_{d,inp} < 1.25$) for $r_1/r_2 \leq 2.5$ but not for $r_1/r_2 \geq 5$. At r_1/r_2 = 0.25, we obtained a binding isotherm with an anomalous shape (Figure S3) and $K_d/K_{d,inp}$ = 1.27. This anomaly was due to a numerical artifact from meshing in COMSOL; by using a more refined mesh, we obtained $K_d/K_{d,inp} < 1.02$. The improvement in accuracy by mesh refinement may suggest that the large deviations in K_d at $r_1/r_2 \geq 5$ are also due to too coarse meshes as well. Thus, more refined and optimized meshes (in particular, for boundary regions between small and large areas) could improve K_d determination in a virtual ACTIS experiment. We confirmed this for the extreme value of r_1/r_2 = 50 and found an optimal $K_d/K_{d,inp}$ = 1.00 at the expense of excessively increasing the computational time (≈72 h instead of ≈3 h) and the potential risk of overfitting (Supporting Information). To keep studies consistent, comparable, and in a reasonable time frame as well as to avoid overfitting, we chose the finer mesh setting from COMSOL without manual optimization for all of the following studies.

It is instructive to analyze the shapes of the separagrams (Figure S3) to understand the influence of varying r_1 on the TIS process. First, for separagrams at r_1/r_2 of up to 2.5 (=250/100), they show the two expected peaks—the first for the nondiffusive species (PL) and the second for the diffusive species (L) as in Figure 1B. However, for greater ratios, i.e., $r_1/r_2 \geq 5$, the two peaks start merging into one (see the shape plots in Figure 5A) followed by a long tail. At these greater ratios, the radius of the injection loop is much larger than that of the separation capillary, and the injection loop length is very short (Table S1). This large difference between the radii causes the sample plug to take more time to move out of the corner regions of the injection loop that are far removed from the center of the axis (Figure S4) during sample injection. Since the motion of the sample plug out of the injection loop is driven not only by convective motion but also by diffusion, more PL is retained in the injection loop as the sample plug is injected into the separation capillary since PL diffuses much slowly than L. This retention causes a significant decrease in the signal of PL (Figure S3). In summary, K_d could be accurately determined for ratios $r_1/r_2 \leq 2.5$. The ratios $r_1/r_2 \geq 5$ resulted in the large deviation in K_d, likely due to a combination of mesh size limitations and nonoptimal TIS conditions; however, it is to be noted that these ratios correspond to r_1 > 500 μm and l_1 < 500 μm, which are impractical parameters for a physical ACTIS instrument.

Variation in Separation Capillary Radius. In this examination, the value of r_2 was varied from 5 to 5000 μm. Thus, the ratio r_2/r_1 (note the ratio is opposite to r_1/r_2 from the previous study) varied from 0.1 (=5/50) to 100 (=5000/50) for a fixed value of r_1 = 50 μm. The rest of the parameters were default (Figure 2B). Note that while the ratios between r_1 and r_2 change in this and the previous examinations, these two sets of virtual experiments are not identical as decreasing r_2, while keeping r_1, l_1, and l_2 constant leads to situations when the plug length is comparable to the length of the separation capillary, which is a greatly suboptimum condition.

For each ratio r_2/r_1, a full set of separagrams has been calculated, and the K_d value was determined from the respective binding isotherm (Figure S5). All determined K_d values were compared to $K_{d,inp}$ (Figure 5B). K_d values were accurate according to our criteria ($0.8 < K_d/K_{d,inp} < 1.25$) for $r_2/r_1 \leq 5$ (=250/50). For r_2/r_1 > 5, the deviation of K_d from $K_{d,inp}$ was beyond the acceptable range; specifically, in this case, the values of K_d were overestimated: $K_d/K_{d,inp} > 1.4$.

Again, it is instructive to analyze the shapes of the separagrams (Figure S5). They show two classical peaks corresponding to the nondiffusive species (PL) and diffusive species (L) (as in Figure 1B) for r_2/r_1 between 1 (=50/50) and 20 (=1000/50). For r_2/r_1 < 1, however, the nondiffusive peak becomes less pronounced (see the left shape plot in Figure 5B), which can be attributed to the plug length ($l_{plug} \geq 52$ cm) being greater than the distance from the capillary inlet to the detection window (l_2 = 50 cm). Consequently, most of PL and L in the equilibrium mixture cannot be separated before they

https://dx.doi.org/10.1021/acs.analchem.0c02405
Anal. Chem. 2020, 92, 11973−11980

reach the detector. Obviously, reducing the plug length by adjusting the injection loop would solve this issue and return these cases to the optimum conditions. Still, K_d deviated from the input $K_{d,inp}$ by less than a factor of 1.25, implying that K_d could be accurately determined from these curves.

For $r_2/r_1 > 5$, both peaks merged into a single diffusive one (see the right shape plot in Figure 5B). Here, the time of separation (≥500 s) is comparable with or greater than the characteristic time of complex dissociation ($\approx 1/k_{off}$ = 1000 s); therefore, the injected sample plug is no longer in the state of equilibrium. Moreover, the transfer flow between the small-radius injection loop and the large-radius separation capillary results in the phenomenon of "flow separation".[15] In this situation, the flow lines are no longer parallel across the whole cross section of the separation capillary. Indeed, recirculation of the flow occurs near the capillary walls (Figure S6) leading to remixing, which affects TIS of L from PL. Additionally, the Péclet number *Pe* for large r_2 (>500 μm) becomes smaller than 40 and suggests that longitudinal diffusion along the separation capillary becomes non-negligible at $r_2/r_1 > 5$ ($Pe \approx 42$; Tables S1 and S2).[16] All of the above nonoptimal conditions, i.e., the departure from equilibrium, the flow separation phenomenon, and significant longitudinal diffusion, likely contribute to the large deviation in K_d from $K_{d,inp}$ at $r_2/r_1 > 5$.

In summary, K_d could be accurately determined for $r_1/r_2 \leq 5$. The ratios $r_1/r_2 \geq 10$ resulted in the large deviation in K_d due to the different nonoptimal conditions described previously and likely due to suboptimal meshing. However, if one works within the range of optimal conditions, which correspond to $r_1/r_2 \leq 5$ in our case, it can be concluded that the accuracy of K_d determination by ACTIS is invariant with respect to changes in the separation capillary radius.

Variation in the Shape of the Initial Plug. For this study, the plug shape was varied ranging from an ideal cylindrical shape to conical shapes and to asymmetrical shapes. Here, as opposed to injecting the plug from the injection loop, the initial plug was defined at the entrance of the separation capillary; no injection process with Q_{inj} was simulated; only the TIS-causing propagation at Q_{TIS} was computed. The variation in concentration distributions in the initial plug was done by changing parameters k_1 and k_2 of the Heaviside function, as illustrated in Figure 3A. The rest of the parameters were default (see Figure 2B). For each plug shape, a full set of separagrams has been calculated, and a K_d value was determined from the respective binding isotherm (Figure S7). All determined K_d values were compared to $K_{d,inp}$ (Figure 5C).

For all examined plug shapes, K_d could be accurately determined, i.e., $0.99 \leq K_d/K_{d,inp} \leq 1.08$. The shapes of the separagrams show the two peaks corresponding to the nondiffusive species (PL) and diffusive species (L) (as in Figure 1B) for all plug shapes. All separagrams were only minimally affected by the variations in the plug shape, demonstrating that ACTIS was robust toward large variations in the plug shape and proving that moderate imperfections in the plug shape expected in real experiments would not affect the accuracy of K_d measurements.

Variation in the Ramp Time of Flow Onset. The ramp time t_{ramp} was varied from 0.10 to 40 s, as illustrated in Figure 2C. The total run time was 60 s with the diffusive peak (L) arriving at the detector between 15 and 30 s. The rest of the parameters were default (see Figure 2B). For each value of t_{ramp}, a full set of separagrams has been obtained, and a K_d value was determined from the respective binding isotherm (Figure S8). All determined K_d values were compared to $K_{d,inp}$ (Figure 5D). For all examined t_{ramp}, K_d could be accurately determined, i.e., $0.97 \leq K_d/K_{d,inp} \leq 1.17$. The shapes of the separagrams show the two peaks corresponding to the nondiffusive species (PL) and diffusive species (L) (as in Figure 1B) for all t_{ramp}. Overall, separagram shapes change only slightly; only positions of the nondiffusive and diffusive peaks move from 10 to 25 s and from 17 to 35 s, respectively (Figure S8). These results show that the accuracy of K_d determination with ACTIS is robust toward changes in the ramp time of the flow onset.

■ CONCLUSIONS

In this work, we examined and proved the robustness of ACTIS, in a virtual fluidic system resembling the one of a real ACTIS instrument, toward large variations in the parameters characterizing both the fluidic system and the flow. We used COMSOL to construct a virtual five-component ACTIS setup, exactly mimicking the geometry of a physical assembly (Figure 2). K_d determined in this setup deviated from $K_{d,inp}$, by a factor of only 1.02.

This five-component ACTIS setup was also used to study how the accuracy of K_d is affected by variations in (i) the radius of the injection loop while keeping its volume constant, (ii) the radius of the separation capillary, (iii) the shape of the initial (prior to the start of TIS) plug of the equilibrium mixture, and (iv) the ramp time in the flow rate onset (after the start of TIS). The variations used in the test exceeded markedly those that could be caused by undesirable variations expected in a physical ACTIS setup. The tested variations provide wide ranges for the desirable experimental instrumental adjustments, which would not make ACTIS inaccurate. In general, the values of K_d did not deviate from the input K_d values by more than a factor of 1.25 upon variations in the above parameters.

Regarding the variation of the injection loop radius, we found that K_d could be accurately determined for $0.05 \leq r_1/r_2 \leq 2.5$. Larger ratios, i.e., $r_1/r_2 \geq 5$, corresponding to injection loop radii much greater than the separation capillary radius resulted in deviations greater than by a factor of 1.25, likely due to a combination of mesh size limitations and nonoptimal TIS conditions.

Accuracy of K_d was also not affected greatly by variation of the separation capillary radius if $r_2/r_1 < 10$. Note that for $r_2/r_1 \leq 0.5$ the signal variation in the separagram becomes much smaller caused by the plug length being comparable to the separation capillary length (Table S2). A small signal variation will make it difficult to evaluate separagrams containing noise, e.g., from experimental data. Great deviations in K_d were observed for $r_2/r_1 \geq 10$ due to the departure from equilibrium of the injected sample plug, the flow separation phenomenon, and significant longitudinal diffusion, with deviation in K_d of $K_d/K_{d,inp} > 1.25$. The mesh size limitations likely also contribute to the observed deviations.

Moreover, deviations in the plug shape from the ideal cylindrical shape do not influence the accuracy of K_d. If plug injection is reproducible from run to run, the determined K_d will be accurate.

Finally, large variations in the pump ramp time for the flow onset do not influence the accuracy in K_d, i.e., cost-effective pumps with slow ramp times can be used for ACTIS.

https://dx.doi.org/10.1021/acs.analchem.0c02405
Anal. Chem. 2020, 92, 11973−11980

From the above results and our experience, we recommend the following strategy to set up an ACTIS instrument. First, one should choose the propagation flow rate (Q_{TIS}) as well as the separation capillary dimensions (r_2 and l_2) so that the ligand L reaches the detector at time τ_L (see eqs 8, 9, and 10), which is much shorter than the anticipated lifetime of the complex ($1/k_{off}$). Our choice of $\tau_L \approx 10$ s should suffice most of the stable PL complexes. Second, the injection loop radius r_1 should be selected to be 0.5−1.0 times the separation capillary radius r_2. For instance, a separation capillary radius of 100 μm corresponds to a range in an injection loop radius of 50−100 μm. Third, the ACTIS instrument should be assembled using the straightforward scheme provided in Figure 2; an elaborate setup proposed in our preliminary study[1] is not needed since parameters such as the plug shape or ramp time have only minimal impact on K_d accuracy according to the results of our current study.

Our findings and recommendations will allow ACTIS-instrumentation developers to change (simplify) instrument configuration drastically without raising questions about how such changes may affect the accuracy of K_d. By relying on ACTIS intrinsic accuracy, developers can focus their efforts and resources on optimizing instrument configuration to achieve the highest precision. Finally, to the best of our knowledge, this work provides the first example of a comprehensive proof of accuracy of an analytical method performed *in silico*. We foresee that the *in silico* accuracy assessment approach will be used for a similar task on other methods built upon processes with the deterministic nature.

■ ASSOCIATED CONTENT

Supporting Information

The Supporting Information is available free of charge at https://pubs.acs.org/doi/10.1021/acs.analchem.0c02405.

> Theoretical background for computer simulation and data evaluation; simulation of separagrams; small ratio of diffusion coefficient (Figure S1); variation in $k_{off,inp}$—separagrams and binding isotherms (Figure S2); variation in injection loop dimensions—separagrams and binding isotherms (Figure S3); variation in injection loop dimensions—sample plug distribution (Figure S4); variation in separation capillary radii—separagrams and binding isotherms (Figure S5); velocity streamlines at different separation capillary radii (Figure S6); variation in the initial plug shape—separagrams and binding isotherms (Figure S7); variation in the ramp time of flow onset—separagrams and binding isotherms (Figure S8); and Péclet number and plug length (Tables S1 and S2) (PDF)

■ AUTHOR INFORMATION

Corresponding Author

Sergey N. Krylov − *Department of Chemistry and Centre for Research on Biomolecular Interactions, York University, Toronto, Ontario M3J 1P3, Canada;* orcid.org/0000-0003-3270-2130; Email: skrylov@yorku.ca

Authors

Jean-Luc Rukundo − *Department of Chemistry and Centre for Research on Biomolecular Interactions, York University, Toronto, Ontario M3J 1P3, Canada*

J. C. Yves Le Blanc − *SCIEX, Vaughan, Ontario L4K 4V8, Canada*

Sven Kochmann − *Department of Chemistry and Centre for Research on Biomolecular Interactions, York University, Toronto, Ontario M3J 1P3, Canada;* orcid.org/0000-0001-7423-4609

Complete contact information is available at: https://pubs.acs.org/10.1021/acs.analchem.0c02405

Author Contributions

The manuscript was written through the contributions of all authors, and all authors have given approval to the final version of the manuscript before the submission.

Notes

The authors declare no competing financial interest.

■ ACKNOWLEDGMENTS

This work was supported by the Natural Sciences and Engineering Research Council of Canada (Grant SPGP 521331-2018).

■ REFERENCES

(1) Sisavath, N.; Rukundo, J.-L.; Le Blanc, J. C. Y.; Galievsky, V. A.; Bao, J.; Kochmann, S.; Stasheuski, A. S.; Krylov, S. N. *Angew. Chem., Int. Ed.* **2019**, *58*, 6635−6639.

(2) Harada, M.; Kido, T.; Masudo, T.; Okada, T. *Anal. Sci.* **2005**, *21*, 491−496.

(3) Okada, T.; Harada, M.; Kido, T. *Anal. Chem.* **2005**, *77*, 6041−6046.

(4) Kanoatov, M.; Galievsky, V. A.; Krylova, S. M.; Cherney, L. T.; Jankowski, H. K.; Krylov, S. N. *Anal. Chem.* **2015**, *87*, 3099−3106.

(5) Pollard, T. D. *Mol. Biol. Cell* **2010**, *21*, 4057−4298.

(6) Jameson, D. M.; Ross, J. A. *Chem. Rev.* **2010**, *110*, 2685−2708.

(7) Wu, P.; Brand, L. *Anal. Biochem.* **1994**, *218*, 1−13.

(8) Umehara, R.; Harada, M.; Okada, T. *J. Sep. Sci.* **2009**, *32*, 472−478.

(9) Taylor, G. I. *Proc. R. Soc. A* **1953**, *219*, 186−203.

(10) Umehara, R.; Miyahara, H.; Okino, A.; Harada, M.; Okada, T. *Anal. Sci.* **2012**, *28*, 359−365.

(11) Kythe, P. K. *Sinusoids: Theory and Technological Applications*; Chapman and Hall/CRC, 2014.

(12) Basile, W.; Salvatore, M.; Bassot, C.; Elofsson, A. *PLoS Comput. Biol.* **2019**, *15*, No. e1007186.

(13) Young, M. E.; Carroad, P. A.; Bell, R. L. *Biotechnol. Bioeng.* **1980**, *22*, 947−955.

(14) Schramke, J. A.; Murphy, S. F.; Doucette, W. J.; Hintze, W. D. *Chemosphere* **1999**, *38*, 2381−2406.

(15) Durst, F. *Fluid Mechanics. An Introduction to the Theory of Fluid Flows*; Springer, 2007.

(16) Chamieh, J.; Leclercq, L.; Martin, M.; Slaoui, S.; Jensen, H.; Østergaard, J.; Cottet, H. *Anal. Chem.* **2017**, *89*, 13487−13493.

SUPPORTING INFORMATION

Assessing Accuracy of an Analytical Method *in silico*: Application to "Accurate Constant *via* Transient Incomplete Separation" (ACTIS)

Jean-Luc Rukundo[1], J.C. Yves Le Blanc[2], Sven Kochmann[1], Sergey N. Krylov[1]

[1]Department of Chemistry and Centre for Research on Biomolecular Interactions, York University, Toronto, Ontario M3J 1P3, Canada
[2]SCIEX, Vaughan, Ontario L4K 4V8, Canada.

Table of Contents Sections

Theoretical background for computer simulation and data evaluation. S-2

Simulation of separagrams S-4

Small ratio of diffusion coefficients – separagrams and binding isotherms S-6

Variation in the input k_{off} – separagrams and binding isotherms S-7

Variation in injection loop dimensions – separagrams and binding isotherms S-8

Variation in injection loop dimensions – sample-plug distribution S-9

Variation in separation capillary radii – separagrams and binding isotherms S-10

Velocity streamlines at different separation capillary radii S-11

Variation in the initial plug shape – separagrams and binding isotherms S-12

Variation in ramp time of flow onset – separagrams and binding isotherms S-13

Péclet number and plug length S-14

Additional supplementary files

The following supplementary files can be found on ChemRxiv (**DOI:** 10.26434/chemrxiv.12345644):

File name	Description/Experiment
evaluation.zip	Evaluation files with raw data.
models.zip	Model files of numerical simulations in COMSOL.

Theoretical background for computer simulation and data evaluation.

Separagrams were simulated with COMSOL in order to assess accuracy and robustness of ACTIS. The following set of partial differential equations describes the simulated processes of longitudinal advection, diffusion, and reversible-binding reaction of L and P forming complex PL:

$$\begin{aligned}
&\frac{\partial[\mathrm{P}]}{\partial t}+v(r)\frac{\partial[\mathrm{P}]}{\partial x}-\mu_{\mathrm{P}}\left(\frac{\partial^2[\mathrm{P}]}{\partial^2 x}+\frac{1}{r}\frac{\partial}{dr}\left(r\frac{\partial[\mathrm{P}]}{dr}\right)\right)=-k_{\mathrm{on,inp}}[\mathrm{P}][\mathrm{L}]+k_{\mathrm{off,inp}}[\mathrm{PL}]\\
&\frac{\partial[\mathrm{L}]}{\partial t}+v(r)\frac{\partial[\mathrm{L}]}{\partial x}-\mu_{\mathrm{L}}\left(\frac{\partial^2[\mathrm{L}]}{\partial^2 x}+\frac{1}{r}\frac{\partial}{dr}\left(r\frac{\partial[\mathrm{L}]}{dr}\right)\right)=-k_{\mathrm{on,inp}}[\mathrm{P}][\mathrm{L}]+k_{\mathrm{off,inp}}[\mathrm{PL}]\\
&\frac{\partial[\mathrm{PL}]}{\partial t}+v(r)\frac{\partial[\mathrm{PL}]}{\partial x}-\mu_{\mathrm{PL}}\left(\frac{\partial^2[\mathrm{PL}]}{\partial^2 x}+\frac{1}{r}\frac{\partial}{dr}\left(r\frac{\partial[\mathrm{PL}]}{dr}\right)\right)=k_{\mathrm{on,inp}}[\mathrm{P}][\mathrm{L}]-k_{\mathrm{off,inp}}[\mathrm{PL}]
\end{aligned} \tag{S1}$$

where, $k_{\mathrm{on,inp}}$ and $k_{\mathrm{off,inp}}$ are rate constants of the reversible binding reaction:

$$\mathrm{P}+\mathrm{L}\underset{k_{\mathrm{off,inp}}}{\overset{k_{\mathrm{on,inp}}}{\rightleftarrows}}\mathrm{PL} \tag{S2}$$

μ is the diffusion coefficient, and $v(r)$ is the parabolic velocity profile of laminar pipe flow described by:

$$v(r)=v_{\max}\left(1-\frac{r^2}{a^2}\right),\quad v_{\max}=2v_{\mathrm{av}} \tag{S3}$$

where a is a capillary radius, $v_{\max}$ is the flow velocity in the capillary centre, and v_{av} is the average flow velocity. The average velocity may be expressed through the volumetric flow rate (Q):

$$v_{\mathrm{av}}=\frac{Q}{\pi a^2} \tag{S4}$$

with:

$$\begin{aligned}
Q=Q_{\mathrm{inj}},&\quad 0<t\le t_1\\
Q=Q_{\mathrm{TIS}}>>Q_{\mathrm{inj}},&\quad t\ge t_2\\
Q_{\mathrm{inj}}<Q<Q_{\mathrm{TIS}},&\quad t_1<t<t_2
\end{aligned} \tag{S5}$$

The initial conditions are:

$$[\mathrm{P}]=0,\quad [\mathrm{L}]=0,\quad [\mathrm{PL}]=0;\quad 0\le x\le l,\quad t=0 \tag{S6}$$

where l is the length of the capillary. The boundary conditions are:

$$\begin{aligned}
&[\mathrm{P}]=[\mathrm{P}]_{\mathrm{eq}},\quad [\mathrm{L}]=[\mathrm{L}]_{\mathrm{eq}},\quad [\mathrm{PL}]=[\mathrm{PL}]_{\mathrm{eq}};\quad x=0,\quad 0<t<t_1\\
&\mu_{\mathrm{P}}\partial_r[\mathrm{P}]=0,\quad \mu_{\mathrm{L}}\partial_r[\mathrm{L}]=0,\quad \mu_{\mathrm{PL}}\partial_r[\mathrm{PL}]=0;\quad r=a,\quad 0<t<t_1\\
&\mu_{\mathrm{P}}\partial_x[\mathrm{P}]=0,\quad \mu_{\mathrm{L}}\partial_x[\mathrm{L}]=0,\quad \mu_{\mathrm{PL}}\partial_x[\mathrm{PL}]=0;\quad x=l,\quad 0<t<t_1
\end{aligned} \tag{S7}$$

and:

$$
\begin{aligned}
&[\mathrm{P}]=0, \quad [\mathrm{L}]=0, \quad [\mathrm{P\text{-}L}]=0; \quad x=0, \quad t>t_1 \\
&\mu_{\mathrm{P}}\partial_r[\mathrm{P}]=0, \quad \mu_{\mathrm{L}}\partial_r[\mathrm{L}]=0, \quad \mu_{\mathrm{PL}}\partial_r[\mathrm{PL}]=0; \quad r=a, \quad t>t_1 \\
&\mu_{\mathrm{P}}\partial_x[\mathrm{P}]=0, \quad \mu_{\mathrm{L}}\partial_x[\mathrm{L}]=0, \quad \mu_{\mathrm{PL}}\partial_x[\mathrm{PL}]=0; \quad x=l, \quad t>t_1
\end{aligned} \tag{S8}
$$

The injected equilibrium mixture contained L, P, and PL at equilibrium concentrations of $[\mathrm{L}]_{\mathrm{eq}}$, $[\mathrm{P}]_{\mathrm{eq}}$, and $[\mathrm{PL}]_{\mathrm{eq}}$, respectively:

$$
[\mathrm{L}]_{\mathrm{eq}} = [\mathrm{L}]_0 - [\mathrm{PL}]_{\mathrm{eq}} \tag{S9}
$$

$$
[\mathrm{L}]_{\mathrm{eq}} = \frac{-([\mathrm{P}]_0 - [\mathrm{L}]_0 + K_{\mathrm{d}}) + \sqrt{([\mathrm{L}]_0 - [\mathrm{P}]_0 + K_{\mathrm{d}})^2 + 4[\mathrm{P}]_0 K_{\mathrm{d}}}}{2} \tag{S10}
$$

$$
[\mathrm{PL}]_{\mathrm{eq}} = \frac{([\mathrm{L}]_0 + [\mathrm{P}]_0 + K_{\mathrm{d}}) - \sqrt{([\mathrm{L}]_0 - [\mathrm{P}]_0 + K_{\mathrm{d}})^2 + 4[\mathrm{P}]_0 K_{\mathrm{d}}}}{2} \tag{S11}
$$

$$
[\mathrm{P}]_{\mathrm{eq}} = [\mathrm{P}]_0 - [\mathrm{PL}]_{\mathrm{eq}} \tag{S12}
$$

where $[\mathrm{L}]_0$ and $[\mathrm{P}]_0$ are initial concentrations of L and P, respectively. Transformations of reactive species (RS) inside the capillary were described with reaction rates RS_{L}, RS_{P}, and RS_{PL}:

$$
RS_{\mathrm{L}} = -k_{\mathrm{on}}[\mathrm{P}][\mathrm{L}] + k_{\mathrm{off}}[\mathrm{PL}] \tag{S13}
$$

$$
RS_{\mathrm{P}} = -k_{\mathrm{on}}[\mathrm{P}][\mathrm{L}] + k_{\mathrm{off}}[\mathrm{PL}] \tag{S14}
$$

$$
RS_{\mathrm{PL}} = k_{\mathrm{on}}[\mathrm{P}][\mathrm{L}] - k_{\mathrm{off}}[\mathrm{PL}] \tag{S15}
$$

Simulation of separagrams

For the simulations we used COMSOL Multiphysics software, version 5.4, with the "Transport of Diluted Species" and "Laminar Flow" modules, which incorporate equations for mass transfer and the reversible binding reaction of P and L in an equilibrium mixture (models are available in **models.zip**). Computation time depends on the dimensions of the simulated geometries; thus, to reduce this time, the lengths of all the five fluidic components were scaled down along with the length of the detection window. The values of Q_{inj} and Q_{TIS} also were scaled down to keep the l_2 / Q_{TIS} ratio constant (see eq 8 in main text). A scale factor of 50 was used. Therefore, for the default ACTIS set up the separation capillary length l_2 was scaled down from 50 cm to 1 cm, the injection loop radius l_1 from 13 cm to 0.26 cm, the connectors lengths from 1.1 mm to 22 µm, the pump tube from 5 cm to 0.1 cm, the TIS propagation flow rate Q_{TIS} from 50 µL / min to 1 µL / min, and the injection flow rate Q_{inj} from 5 µL/min to 0.1 µL / min. For all the simulations a mesh distribution calibrated for fluid dynamics was used with a "*finer mesh*" size setting to optimize the accuracy with respect to computational time and memory requirements; the simulation times where ≈ 3 h (2 × Intel® Xenon® CPU X5690@3.47 GHz, 96 GB RAM). A more refined mesh size setting *i.e.* "*extra fine mesh*" was tested but resulted in a much longer simulation time of ≈ 20 h.

In all virtual experiments, we considered a small-molecule L with typical diffusion coefficient of $\mu_L = 500$ µm²/s and a large P with a typical diffusion coefficient of $\mu_P = 50$ µm²/s. The remaining parameters were: $k_{on,inp} = 10^3$ M^{-1}s^{-1}, $k_{off,inp} = 10^{-3}$ s^{-1}, $K_d = k_{off,inp} / k_{on,inp} = 10^{-6}$ M^{-1}, $\mu_{PL} = \mu_P = 50$ µm²/s, $[L]_0 = 0.5$ µM, $T = 300$ K. $[P]_0$ was varied from 1 nM to 1 mM using 11 different non-zero concentrations plus zero concentration. Three other values of $k_{off,inp}$ *i.e.* 10^{-4}, 10^{-5}, and 10^{-6} s^{-1} with respective values of $K_{d,inp}$, 10^{-7}, 10^{-8}, and 10^{-9} M, were also used in COMSOL (**variation_Kd.mph** in **models.zip**).

Variations in the injection loop dimensions simulations

The injection loop radius was varied from 5 µm to 5000 µm, with respect to the radius of the separation capillary r_2 which was kept constant at 100 µm (**variation_injection_loop.mph** in **models.zip**). The injected volume (0.02 µL) was kept constant by varying the scaled injection loop length l_2 from 2.6×10^{-5} to 25 cm. The sample-plug injection was done with a flow rate of 0.1 µL / min during 12 s resulting in a plug of approximately 0.6 mm in length inside the separation capillary. Subsequently, a water plug was injected into the capillary with 0.1 µL / min during 12 s to slowly displace the sample-plug from the capillary inlet (plug end distance from the capillary inlet was approximately 0.6 mm). See Table S1 for injection loop lengths at different r_1 / r_2. The simulations at $r_1 / r_2 = 0.25$ were redone using a much refined mesh *i.e.* the "*extra fine mesh*" setting to verify if the factor $K_d / K_{d,inp} = 1.27$ in deviation was due to a numerical artifact. With the refined mesh we obtained an improved factor in deviation of $K_d / K_{d,inp} = 1.02$. Moreover, simulations were also redone with more refined meshes to investigate the influence of mesh resolution on the results. The standard "*extra fine mesh*" setting for $r_1 / r_2 = 5$, 10, and 50 resulted in a $K_d / K_{d,inp}$ deviation of 0.64, 0.40, and 0.24 respectively. This is comparable to the $K_d / K_{d,inp}$ obtained with the regular "*finer mesh" i.e.* 0.66, 0.44 and 0.15 for $r_1 / r_2 = 5$, 10, and 50 respectively. However, results could be improved for $r_1 / r_2 = 50$ by careful and manual optimization of the mesh parameters in COMSOL (**variation_injection_loop_refined_mesh.mph** in **models.zip**). This manual mesh optimization resulted in an optimal K_d / $K_{d,inp} = 1.00$ but increased the computational time by a factor of 24 (from 3 h to 72 h). This optimal result of K_d / $K_{d,inp} = 1.00$ also indicates the great risk of heavy manual mesh optimization, *i.e.* overfitting (changing the COMSOL model parameters until K_d fits $K_{d,inp}$

perfectly). To avoid this risk, we chose the regular "*finer mesh*" setting from COMSOL without manual optimization for all following studies.

Variation in the separation capillary diameter simulations

The separation capillary radius r_2, was varied from 5 µm to 5000 µm, with respect to the radius of the injection loop r_1 which was kept constant at 50 µm (**variation_separation_capillary.mph** in **models.zip**). The sample-plug injection was done with a flow rate of 0.1 µL / min during 12 s. Subsequently, a water plug was injected into the capillary with 0.1 µL / min during 12 s to slowly displace the sample-plug from the capillary inlet (plug end distance from the capillary inlet was approximately 0.6 mm). The scaled sample-plug lengths inside the separation capillary varied from 25 cm to 2.6×10^{-5} cm. Note that the scaled length of the separation capillary was 1 cm. Therefore, for $r_2 / r_1 < 1$ the sample-plug lengths are longer or equal in length to separation capillary which causes the sample-plug to exit the separation capillary during the sample-plug injection and slow displacement steps. See Table S2 for sample-plug lengths inside separation capillary at different r_2 / r_1.

Variation in the initial plug shape simulations

The plug shape was represented as a square wave function and defined as an analytical function in COMSOL (**variation_plug_shape.mph** in **models.zip**). The simulations were done with our default ACTIS setup. The sample-plug concentration distribution was varied by changing the parameters k_1 and k_2 as explained in the main text. For this study the plug was defined at the entrance of the separation capillary as opposed to the injection loop. Here, a water plug was injected into the capillary with 0.1 µL / min during 12 s to slowly displace the sample-plug from the capillary inlet (plug end distance from the capillary inlet was approximately 0.6 mm).

Variation in ramp time of flow onset simulations

The ramp time was defined by a step function in COMSOL (**variation_ramp_time.mph** in **models.zip**). The transition zone from the injection flow rate Q_{inj} and Q_{TIS} was varied from 0.1 to 40 s. The simulations were done with our default ACTIS setup. The sample-plug injection was done with a flow rate of 0.1 µL / min during 12 s resulting in a plug of approximately 0.6 mm in length. Subsequently, a water plug was injected into the capillary with 0.1 µL / min during 12 s to slowly displace the sample-plug from the capillary inlet (plug end distance from the capillary inlet was approximately 0.6 mm). The ratio between the injection loop and the separation capillary was set to one $r_1 / r_2 = 1$.

Small ratio of diffusion coefficients

A small protein with $\mu_P = 110$ µm²/s and a small molecule with $\mu_L = 300$ µm²/s were used to assess the effect of a small ratio of diffusion coefficient, *i.e.* $\mu_L/\mu_p \approx 3$, and compare this small ratio to the default ratio ($\mu_L = 500$ µm²/s, $\mu_{PL} = 50$ µm²/s, *i.e.* $\mu_L/\mu_p = 10$) used in all other studies of this work. The default ACTIS set up dimensions reported in the *Simulations of Separagrams* section above were used and not further optimized for the small ratio. A TIS propagation flow rate of $Q_{TIS} \approx 28$ µL / min was determined using eq. 8 in the main text, and a same injection flow rate $Q_{inj} = 5$ µL/min was used. The flow rates were scaled to $Q_{TIS} \approx 0.6$ µL / min and $Q_{inj} = 0.1$ µL/min in the simulation. The remaining parameters were: $k_{on,inp} = 10^3$ M^{-1}s^{-1}, $k_{off,inp} = 10^{-3}$ s^{-1}, $K_d = k_{off,inp} / k_{on,inp} = 10^{-6}$ M^{-1}, $[L]_0 = 0.5$ µM, $T = 300$ K. $[P]_0$ was varied from 1 nM to 1 mM using 11 different non-zero concentrations plus zero concentration.

Small ratio of diffusion coefficients – separagrams and binding isotherms

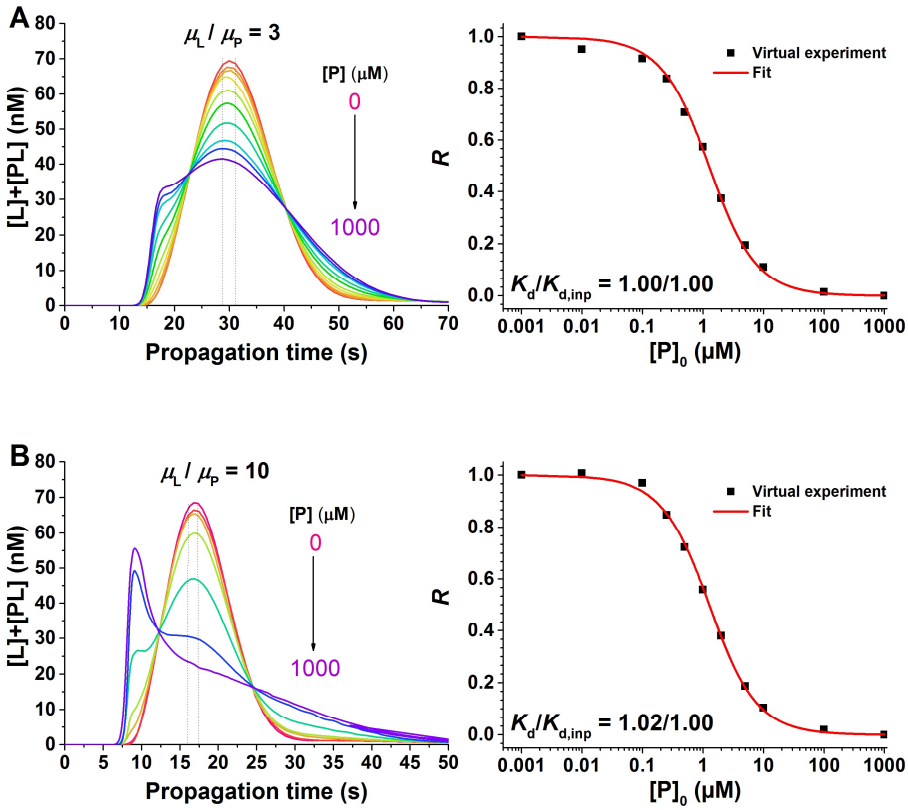

Figure S1. Separagrams and respective binding isotherms at two different ratios of the diffusion coefficient $\mu_L/\mu_P \approx 3$ (μ_L = 300 μm²/s, μ_P = 110 μm²/s) (**A**) and $\mu_L/\mu_P = 10$ (μ_L = 500 μm²/s, μ_P = 50 μm²/s) (**B**). The separation at $\mu_L/\mu_P \approx 3$ and $\mu_L/\mu_P = 10$ differ somewhat in peak resolution where the complex peak at $\mu_L/\mu_P \approx 3$ is not as pronounced compared to $\mu_L/\mu_P = 10$. The deviation at $\mu_L/\mu_P \approx 3$ was insignificant, *i.e.* $K_d / K_{d,inp} = 1.00$, which is consistent with the deviation of $K_d / K_{d,inp} = 1.02$ gained with $\mu_L/\mu_P \approx 10$.

Variation in the input k_{off} – separagrams and binding isotherms

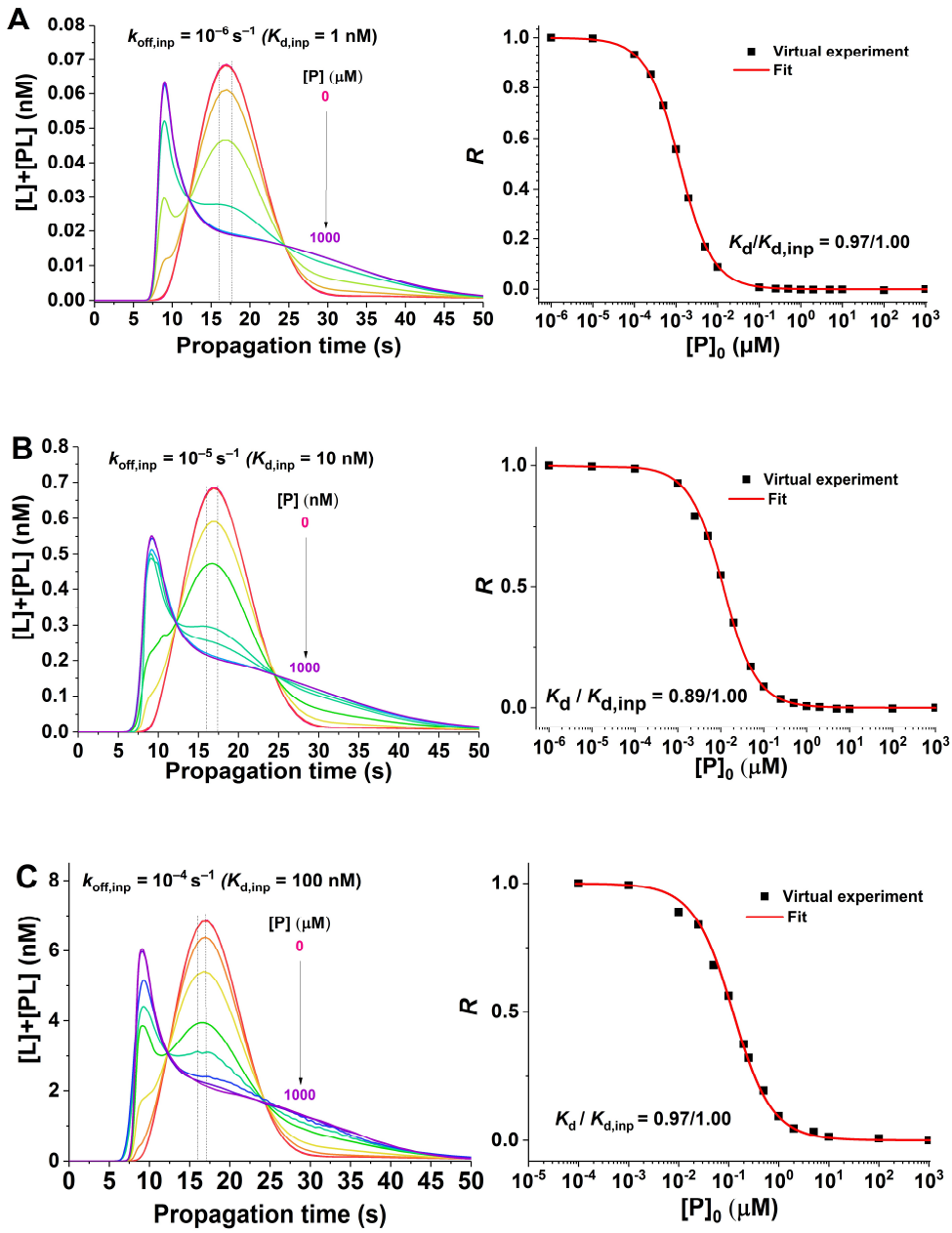

Figure S2. Separagrams and respective binding isotherms for different additional $k_{off,inp}$. The additional values of $k_{off,inp}$ were 10^{-4}, 10^{-5}, and 10^{-6} s^{-1} with respective values of $K_{d,inp}$: 10^{-7}, 10^{-8}, and 10^{-8} M. The deviation at those different k_{off} was $K_d / K_{d,inp} < 1.1$ which is consistent with the deviation of $K_d / K_{d,inp} = 1.02$ gained with the standard $k_{off,inp} = 10^{-3}$ s^{-1} ($K_{d,inp} = 10^{-6}$ M, see Figure 4 in the main text) that was used in all other simulations.

Variation in injection loop dimensions – separagrams and binding isotherms

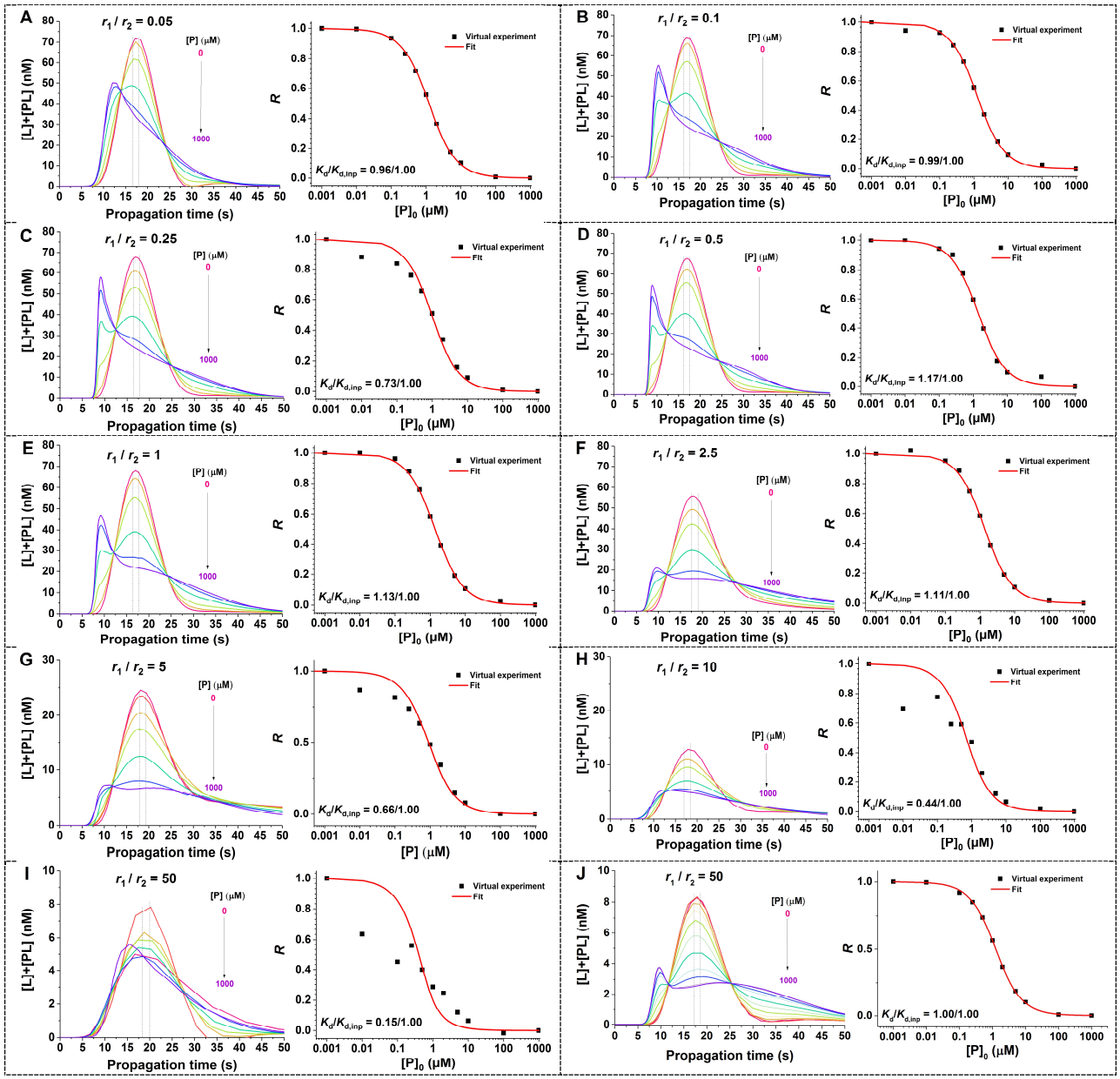

Figure S3. Separagrams and respective binding isotherms at different injection loop radii r_1 with respect to a fixed separation capillary radius r_2. The value of r_1 is varied from 5 μm to 5000 μm, with r_2 = 100 μm. *i.e.* r_1 / r_2 varies from 0.05 (= 5 / 100) to 50 (= 5000 / 100). The scaled length of the injection loop l_1 was varied from 2.6×10^{-5} cm to 2.6×10^{1} cm to keep the volume of the injected sample constant. For $r_1 / r_2 > 2.5$ (**G**, **H**, and **I**) more of the PL is retained in the injection loop (see Figure S4) which shown by the decrease in the height of the complex peak. The study in **J** is the same as in **I** but with an optimized and refined mesh showing that mesh optimization improves the K_d determination.

Variation in injection loop dimensions – sample-plug distribution

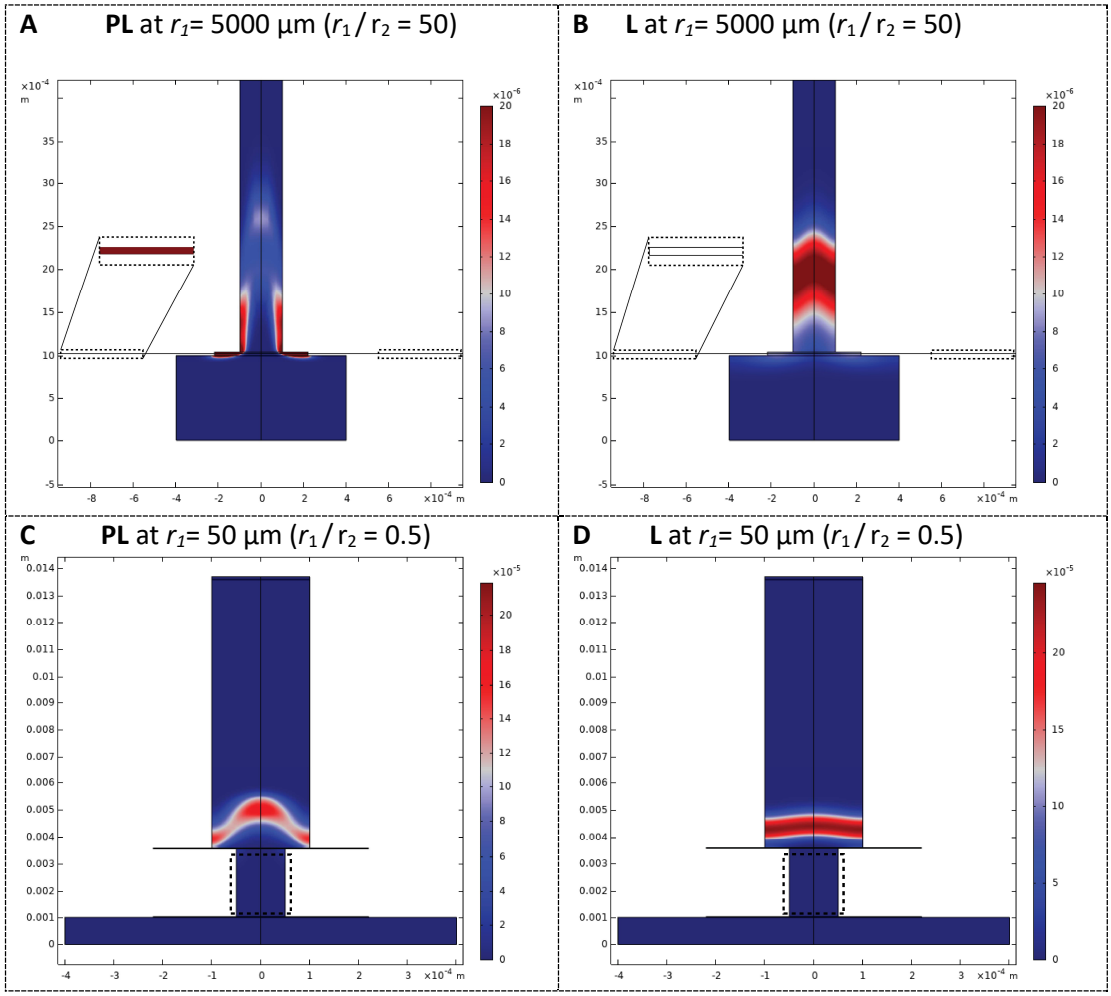

Figure S4. Schematic of the virtual ACTIS instrument at $r_1 / r_2 = 50$ (r_1 = 5000 µm, r_2 = 100 µm) (**A** and **B**) and $r_1 / r_2 = 0.5$ (r_1 = 50 µm, r_2 = 100 µm) (**C** and **D**). The color legend represents the concentration distribution of the injected sample-plug (blue = low concentration, red = high concentration, white = medium concentration). The schematic shows the injection of the complex PL (**A** and **C**) and ligand L (**B** and **D**) right after the slow displacement of the sample-plug step explained in the "Variations in the injection loop dimensions simulations" section. At $r_1 / r_2 = 50$ after injection and displacement, high concentrations of PL are still in the corner regions (dotted rectangle in **A**) of the injection loop as shown by the zoomed in area in **A**. In contrast, PL is completely injected for $r_1 / r_2 = 0.5$ and nothing remains in the injection loop (dotted rectangle in **C**). For $r_1 / r_2 = 50$ a small concentration of L remains in the corner regions of the injection loop (dotted rectangle in **B**). For $r_1 / r_2 = 0.5$, L is fully injected from the injection loop (dotted rectangle in **D**). Notice that for panels **A** and **B** the whole length of the injection loop is not shown for better visibility.

Variation in separation capillary radii – separagrams and binding isotherms

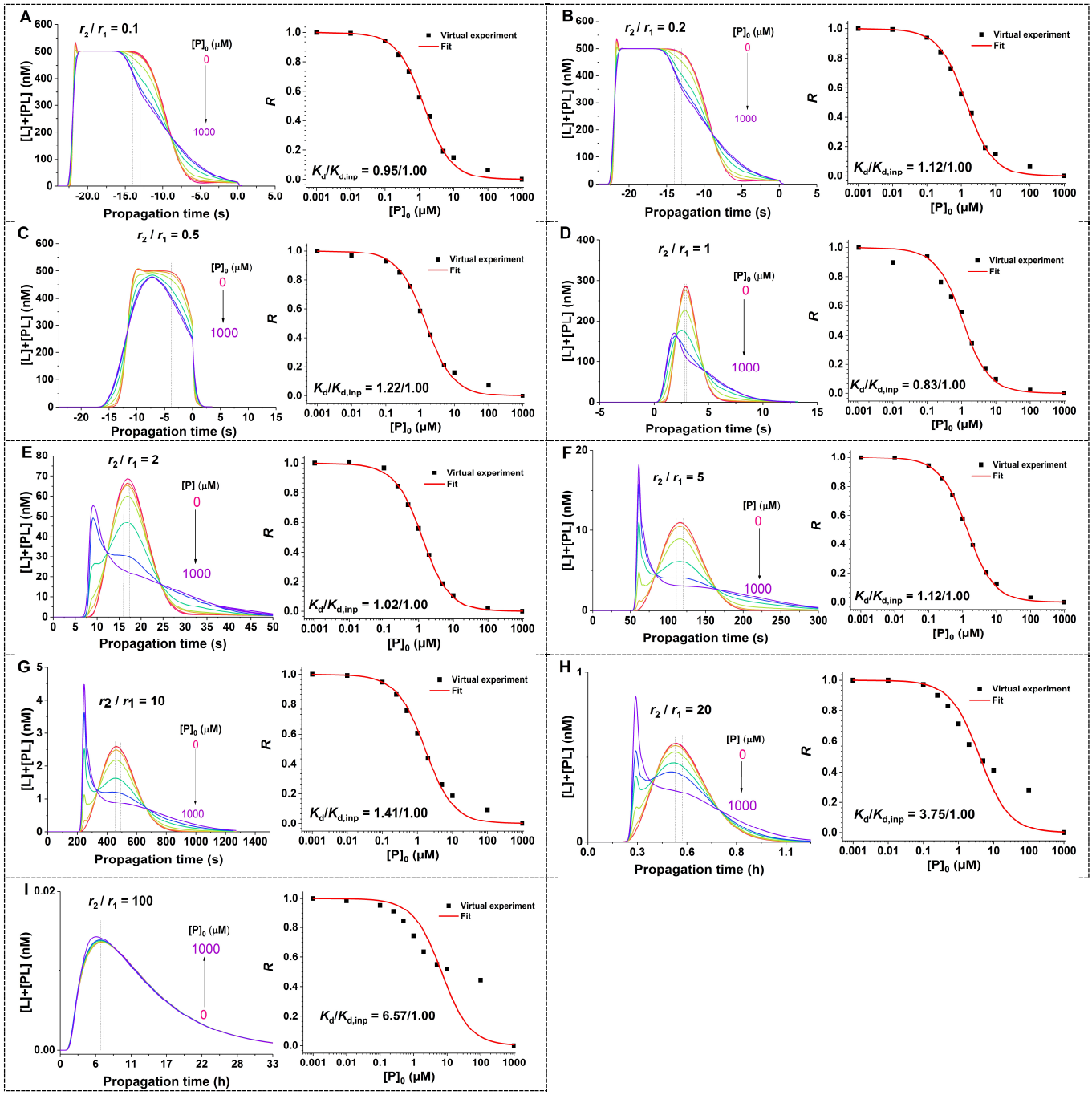

Figure S5. Separagrams and respective binding isotherms at different separation capillary radii r_2 with respect to a fixed injection loop radius r_1. r_2 is varied from 5 μm to 5000 μm, with $r_1 = 50$ μm *i.e.* r_2 / r_1 varies from 0.1 (= 5/50) to 100 (= 5000/50). For $r_2 / r_1 < 1$ (**A**, **B**, and **C**) the propagation times are negative since the plug length is much longer or comparable in the length to the separation capillary and, therefore, the sample elutes during the injection step. For $r_2 / r_1 > 5$ (**G**, **H**, and **I**) the combination of significant longitudinal diffusion, recirculation phenomenon (see Figure S7), and the departure from equilibrium of the injected sample-plug results in a larger deviation of K_d. Notice that at $r_2 / r_1 = 100$ (**I**) the time scale for the propagation is in hours.

Velocity streamlines at different separation capillary radii

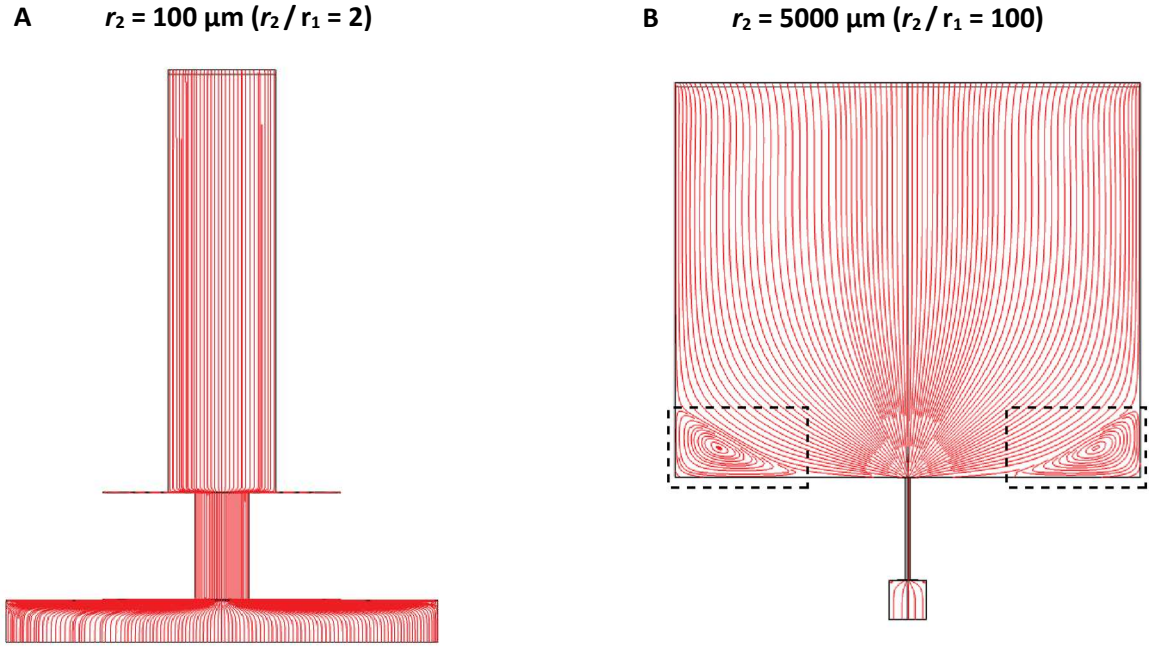

Figure S6. Velocity streamlines at $r_2 / r_1 = 2$ (**A**) and $r_2 / r_1 = 100$ (**B**). At $r_2/r_1 = 2$ the streamlines are parallel in the separation capillary, while at $r_2 / r_1 = 100$ flow recirculation becomes significant at the corners of the separation capillary (dotted regions in **B**).

Variation in the initial plug shape – separagrams and binding isotherms

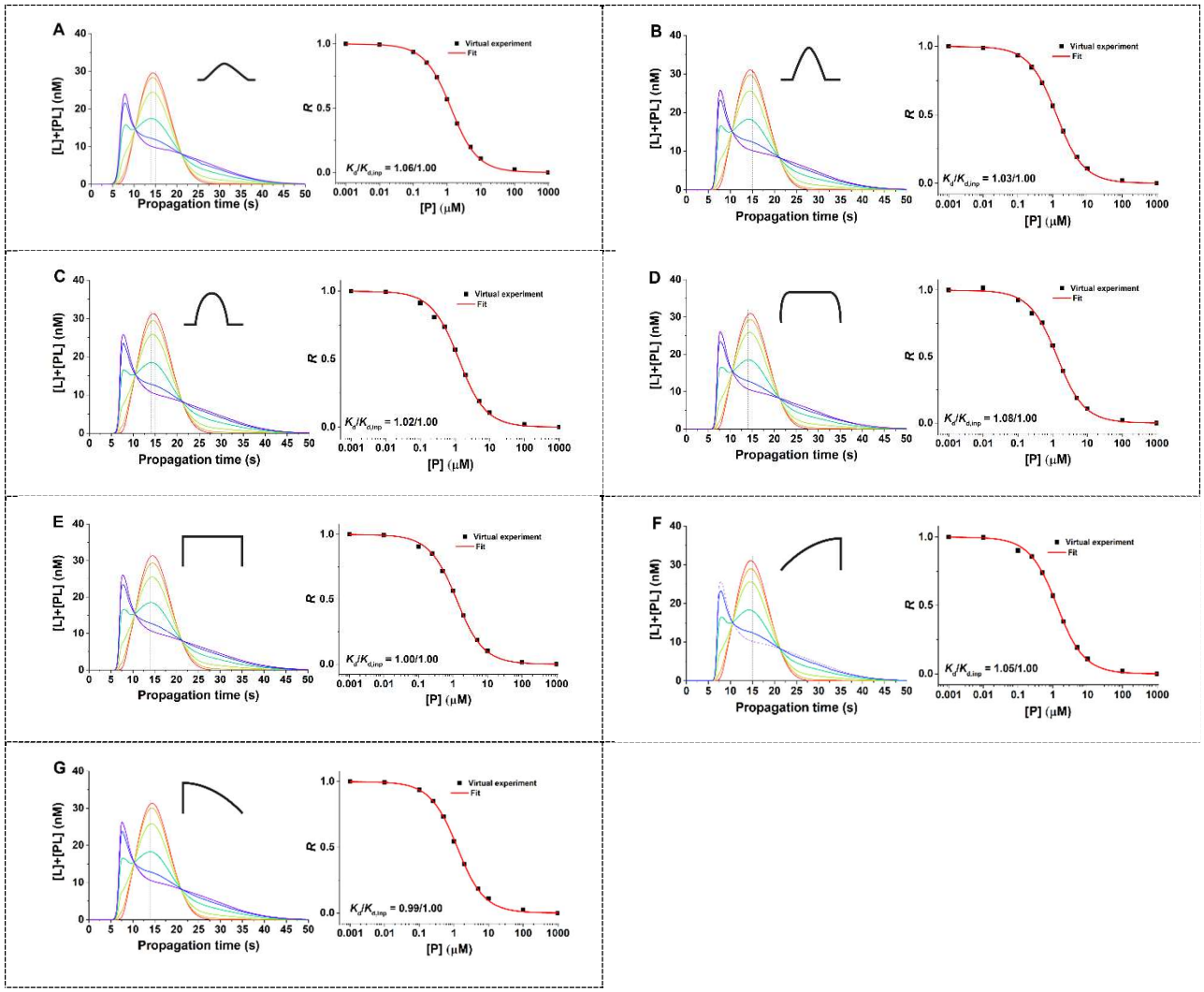

Figure S7. Separagrams and respective binding isotherms at different initial sample-plug concentration distribution (top right corner of each separagram plot). Each sample-plug shape is modeled using a square wave function as explained in the main text and in the section "Variation in the initial plug shape simulations". The separagrams are not affected by the sample-plug shape.

Variation in ramp time of flow onset – separagrams and binding isotherms

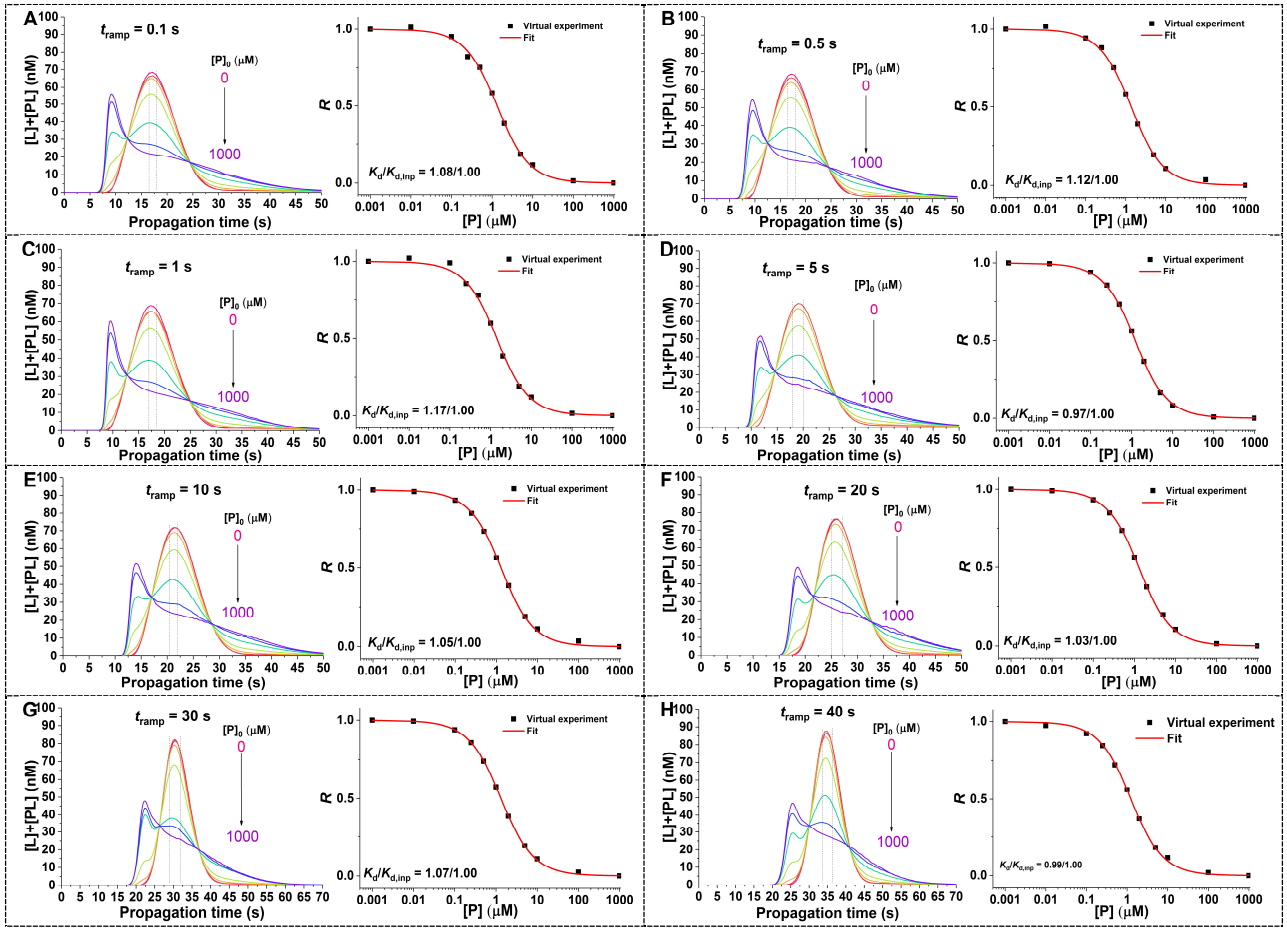

Figure S8. Separagrams and respective binding isotherms at different ramp time of flow onset. Here the ramp time is varied from 0.10 s to 40 s (**A** to **H**). For comparison, the overall runtime of ACTIS is relatively short (peaks of PL and L are detected within 30 s). The shapes of the separagrams are not affected by the change in ramp time. However, the positions of the non-diffusive and diffusive peaks move from 10 to 25 s and from 17 to 35 s with increasing ramp time (from **A** to **H**).

Péclet number and plug length

Table S1. Péclet numbers and plug lengths for variation in injection loop radius.

Radius ratios (r_1/r_2) with r_2 = 100 µm	**Péclet number**	**Scaled Plug length inside separation capillary (cm)**	**Scaled Separation capillary length l_2 (cm)**	**Scaled Loop length l_1 (cm)**
50	106	0.06	1	2.6×10^{-5}
10	106	0.06	1	6.3×10^{-4}
5	106	0.06	1	2.6×10^{-3}
2.5	106	0.06	1	1.0×10^{-2}
1	106	0.06	1	6.4×10^{-2}
0.5	106	0.06	1	2.6×10^{-1}
0.25	106	0.06	1	1.0×10^{0}
0.1	106	0.06	1	6.4×10^{0}
0.05	106	0.06	1	2.6×10^{1}

Table S2. Péclet numbers and plug lengths for variation in separation capillary radius.

Radius ratios (r_2/r_1) with r_1 = 50 µm	**Péclet number**	**Scaled Plug length inside separation capillary (cm)**	**Scaled Separation capillary length l_2 (cm)**	**Scaled Loop length l_1 (cm)**
100	2	2.6×10^{-5}	1	2.6×10^{-1}
20	11	6.4×10^{-4}	1	2.6×10^{-1}
10	21	2.6×10^{-3}	1	2.6×10^{-1}
5	42	1.0×10^{-2}	1	2.6×10^{-1}
2	106	6.4×10^{-2}	1	2.6×10^{-1}
1	212	2.6×10^{-1}	1	2.6×10^{-1}
0.5	424	1.0×10^{0}	1	2.6×10^{-1}
0.2	1061	6.4×10^{0}	1	2.6×10^{-1}
0.1	2122	2.6×10^{1}	1	2.6×10^{-1}